Superlattices and Microstructures 106 (2017) 58–66

Contents lists available at ScienceDirect

Superlattices and Microstructures

journal homepage: www.elsevier.com/locate/superlattices

Influence of defect luminescence and structural modification on the electrical properties of Magnesium Doped Zinc Oxide Nanorods

B. Santoshkumar [a], Amrita Biswas [b], S. Kalyanaraman [a, *], R. Thangavel [c], G. Udayabhanu [b], G. Annadurai [d], S. Velumani [e]

[a] PG and Research Dept. of Physics, Sri Paramakalyani College, Alwarkurichi, 627 412, India
[b] Dept. of Applied Chemistry, Indian Institute of Technology, Dhanbad, 826 004, India
[c] Solar Energy Research Laboratory, Dept. of Applied Physics, Indian Institute of Technology, Dhanbad, 826 004, India
[d] Nanoscience Division, Sri Paramakalyani Centre for Environmental Sciences, Manonmaniam Sundaranar University, Alwarkurichi, 627 412, India
[e] Dept. of Electrical Engineering (SEES), CINVESTAV-IPN, Av. Instituto Politecnico Nacional, # 2508, Col. San Pedro Zacatenc, 07360, Mexico D.F., Mexico

ARTICLE INFO

Article history:
Received 7 January 2017
Received in revised form 19 March 2017
Accepted 22 March 2017
Available online 25 March 2017

Keywords:
Mg doped ZnO nanorod
Hydrothermal method
Electrical transport
Optical properties
Electrochemical impedance spectroscopy

ABSTRACT

Magnesium doped zinc oxide nanorod arrays on zinc oxide seed layers were grown by hydrothermal method. X-ray diffraction (XRD) patterns revealed the growth orientation along the preferential (002) direction. The hexagonal morphology was revealed from the field emission scanning electron microscope (FESEM) images. The elemental composition of the samples was confirmed by energy dispersive x-ray analysis spectra (EDS) and mapping dots. Carrier concentration, resistivity and mobility of the samples were obtained by Hall measurements. *I-V* characteristic curve confirmed the increase in resistivity upon doping. Photoluminescence (PL) spectra exposed the characteristic of UV emission along with defect mediated visible emission in the samples. Electrochemical impedance spectroscopy and cyclic voltammetry were undertaken to study the charge transport property. Owing to the change in the structural parameters and defect concentration the electrical properties of the doped samples were altered.

1. Introduction

One of the nifty materials in the family of semiconductors is the Zinc oxide (ZnO) which has a direct bandgap (3.37 *eV*) and large exciton binding energy (60 *meV*). Owing to its versatility, ZnO is finding its application in the fields of electronics [1], optoelectronics [2], sensing materials [3], and being used as gas sensors [4], photo diodes [5], light emitting diodes [6], photonic crystals [7], photo detectors [8] etc. As a result of its significant fundamental physical properties and applications to several nanostructured devices, ZnO has a multitude of interest in its low dimensional structures like thin film, nanorod, nano wire, nanoparticle, nanotube etc. [9–13]. To fabricate the above said structures various methods such as thermal evaporation, chemical vapour deposition, metal organic chemical vapour deposition, hydrothermal technique were used [14–17]. One

* Corresponding author.
E-mail address: mayura_priya2003@yahoo.co.in (S. Kalyanaraman).

http://dx.doi.org/10.1016/j.spmi.2017.03.039
0749-6036/

dimensional ZnO are the reliable building blocks to manufacture nanoscale optoelectronic, photonic devices and circuits [18–20].

The structural, optical and electrical properties of ZnO can be tuned by doping with various elements in order to make use of ZnO in the above said device applications. Some of the doping elements investigated were Al, Ag, La, Na, Li, In, Ca, Y etc. [21–28]. One of the frequently doped materials in ZnO is Mg. Its structural, optical, magnetic, dielectric [29–34] properties were already undertaken. Sanghyun Ju et al. [35] discussed the application of MgZnO multiple nanorods as n-type FET. MgZnO nanorods were also used as deep UV photodetectors [36–39]. Mg doped ZnO grown by spray [40] and sol-gel [41] method reveal the decrease in electrical properties while increasing the Mg dopant concentration. But none of them gave a conclusive evidence of its electrical properties. It is important to uncover the cause for this variation so as to tailor them efficiently for a specific application.

In our present study, we emphasize on how the electrical properties are varying upon changes in structure and defect concentration in MgZnO nanorods grown by the mild mean hydrothermal technique.

2. Materials and methods

Soda lime glasses were used as substrates. At first ZnO seed layers were grown on the glass substrates by sol-gel spin coating method. The fabrication of ZnO seed layers was given elsewhere [42,43]. ZnO nanorods were grown on these seed layers by hydrothermal method. The precursors for preparing nanorod were zinc nitrate hexahydrate ($Zn(NO_3)_2 \cdot 6H_2O$), hexamethylene tetramine (HMT, $C_6H_{12}N_4$) and Magnesium nitrate hexahdrate ($Mg(NO_3)_2 \cdot 6H_2O$). All precursors were bought from Sigma Aldrich and used without further purification. Magnesium was doped at different percentages such as 0 mol%, 5 mol%, 10 mol% and 15 mol% in the milieu of ZnO. The procedure to prepare the nanorod was elaborately given in our previous work [44]. The samples were characterized by PANalytical X'Pert-PRO x-ray diffractometer with $CuK\alpha_1$ (1.5406 Å) monochromatic radiation to get the structural insights. Using field emission scanning electron microscope (Zeiss Auriga 39-16) the surface morphology and the elemental analyses from the Energy Dispersive X-ray Spectra and mapping dots were obtained. Hall measurements were done using Ecopia HMS −5000 instrument. *I-V* characteristics were studied at room temperature using Keithley 2450 sourcemeter. The photoluminescence measurements were performed at room temperature using Jobin–Yvon LabRAM HR 800UV micro-Raman system with 325 nm line of a He–Cd laser as excitation source. Impedance spectroscopy and cyclic voltammetry have been performed using CHI660C electrochemical workstation.

3. Results and discussion

The XRD patterns of undoped, 5 mol%, 10 mol% and 15 mol% Mg doped ZnO nanorods were shown in Fig. 1. The three major peaks appeared in the XRD patterns which belong to the (100), (002) and (101) directions of ZnO hexagonal wurtzite structure

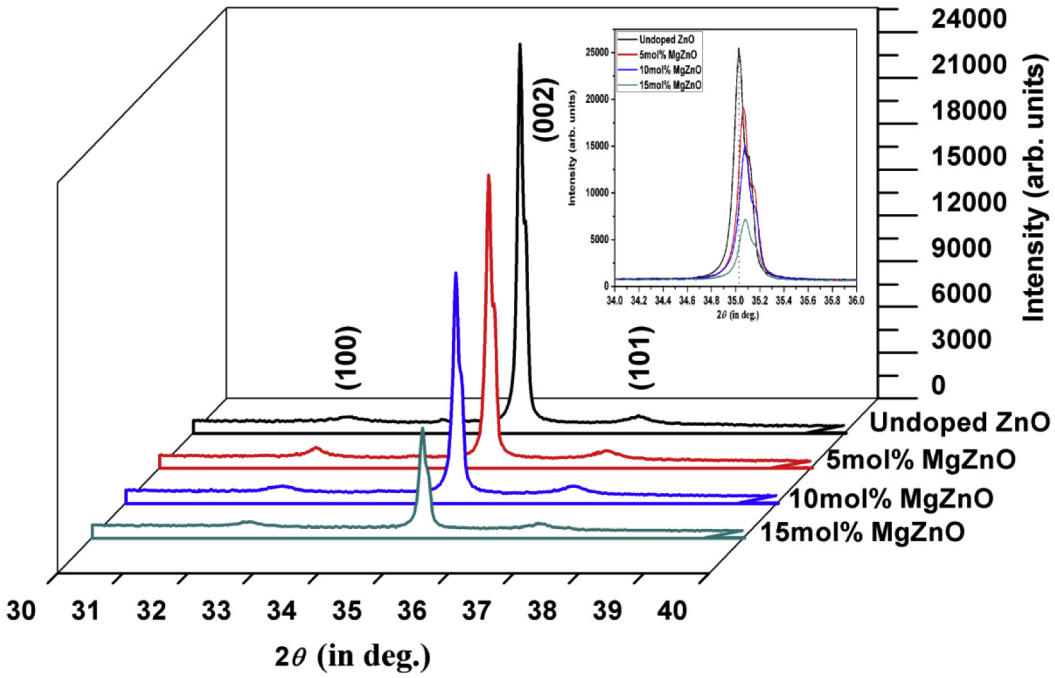

Fig. 1. XRD patterns with (100), (002) and (101) peaks taken within the range 30°–40° Inset indicates the (002) peak shift.

Table 1
Structural parameters calculated from XRD patterns.

Magnesium doping conc. in ZnO (mol%)	FWHM of *(002)* peak (deg.)	Crystallite size *D* (nm)	*a* (Å)	*c* (Å)	*c/a*	Volume *V* (Å)^3
0	0.121	71.91	3.1838	5.1176	1.6074	44.9250
5	0.127	68.52	3.1842	5.1124	1.6056	44.8907
10	0.139	62.60	3.1845	5.1109	1.6049	44.8860
15	0.144	60.43	3.1847	5.1102	1.6046	44.8855

and were associated with the JCPDS card no. 36-1451. The (002) peak was having the maximum intensity due to the lower surface energy of (002) plane in ZnO [45]. Therefore the preferential growth orientation was developed into (002) crystallographic direction and hence the formation of *c*-axis orientation [46]. It was found that as the Mg concentration was increased from 0% to 15%, the position of XRD peaks were shifted towards higher angle side from 35.040° to 35.092° [inset of Fig. 1] due to the smaller ionic radius of the dopant with the host parent atom (ionic radius of $Mg^{2+} = 66$ p.m. and $Zn^{2+} = 74$ p.m.) [47]. This small difference in ionic radii and the similarity in charge states (Mg^{2+} and Zn^{2+}) caused the Mg dopant to be present in the substitution position. When the Zn^{2+} ions were replaced by Mg^{2+} ions the lattice parameters were affected. The calculated structural parameters were scheduled in Table 1. There was an upsurge in the lattice parameter *a* and shrinkage in *c*. The *c/a* axial ratio decreased from 1.6074, 1.6056, 1.6049 and to 1.6046 upon Mg doping. Moreover there was a change in volume between undoped and Mg doped ZnO. This kind of crystal geometry modifications may lead to ionic character [48]. The mean crystallite sizes were calculated using Scherrer's formula $D = 0.9\lambda/\beta \cos\theta$ [49], where $\lambda = 1.5406$ Å for $CuK\alpha_1$ radiation, β is the FWHM and θ is the Bragg angle. The mean crystallite size was found to decrease from 71.91, 68.52, 62.60 and to 60.43 nm by incorporating Mg dopants into the ZnO nanorods. Fig. 2 shows a relationship between crystallite size, FWHM and doping percentage. The dopant Mg atoms accumulated near the boundary of ZnO during growth. When the concentration of dopant was increased, the diffusion rate was reduced and it led to the suppression of the growth of the crystallite and a possible reduction in the size of the particle [50]. The accumulation of Mg atoms and the corresponding size reduction of the particle at the grain boundary increased the scattering which suppressed the intensity of XRD patterns. This may conclude the reduction of crystallinity in the doped samples.

The FESEM images of the as-grown nanorods were shown in Fig. 3. They were hexagonal in shape with *c*-axis perpendicular to the surface of the substrate, consistent with the XRD data. The mean diameters of the nanorods were about 80, 84, 110, and 114 nm for 0 mol%, 5 mol%, 10 mol% and 15 mol% MgZnO respectively. The atomic % of the as-grown nanorods corresponding to different mole concentration of Mg was obtained through EDX and has been given in the inset of Fig. 3. It is indicated that the prepared samples were composed of Zn, Mg and O atoms. It was found that the atomic percentage increased with increasing Mg concentration during the growth of nanorods. EDX images of O, Mg, and Zn elemental mapping dots for sample 5 mol% Mg doping were depicted in Fig. 4. The subdivisions of elements were clearly seen.

Hall measurements were made at room temperature. We have adopted the technique used by R. Thangavel et al. [51]. Since the work function of ZnO (5.3 eV) and Au (5.2 eV) is more or less same the samples were placed directly in the sample holder and the four gold coated Hall probes were placed at the corners in Vander Pauw configuration. The resistance linearity is checked for ohmic nature of the contacts by setting proper current limit. The parameters determined were listed in Table 2. All the samples were *n*-type in character. The room temperature resistivity of the samples increased as a result of increasing donor ionization energy [52]. The activation energy of the donors increased because Mg doping shifted the conduction band away from the intrinsic shallow donor state [53]. Formation of smaller crystallites steered to increase the scattering

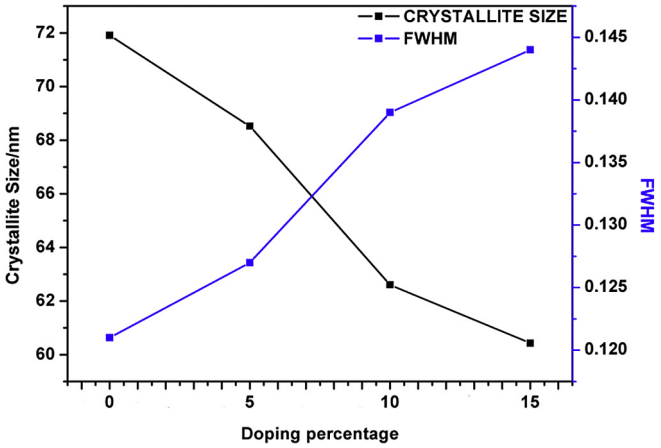

Fig. 2. Variation of crystallite size and FWHM with doping percentage.

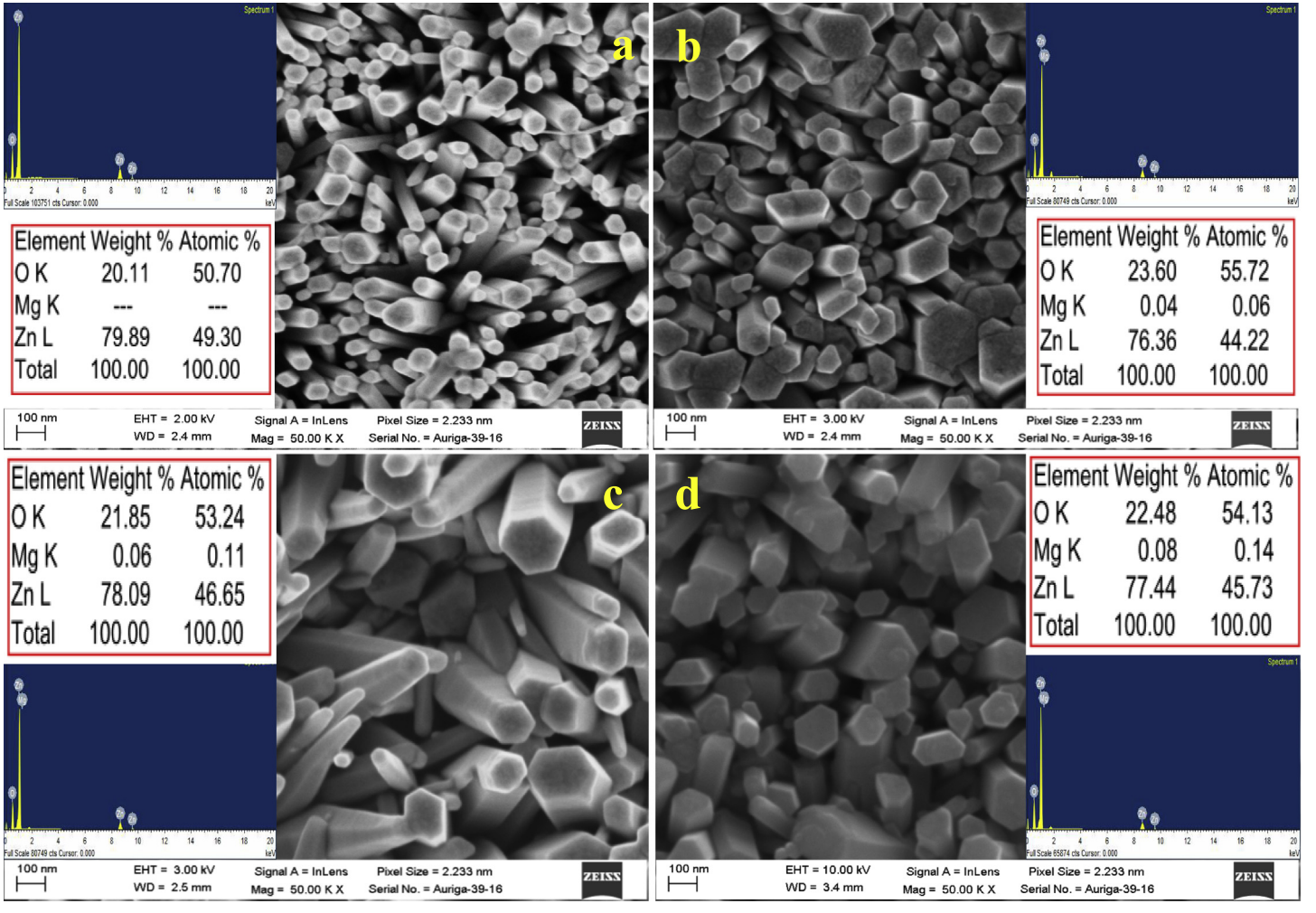

Fig. 3. FESEM images of (a) Undoped (b) 5 mol% (c) 10 mol% and (d) 15 mol% Mg doped ZnO nanorods Inset shows the respective EDX spectra with atomic %.

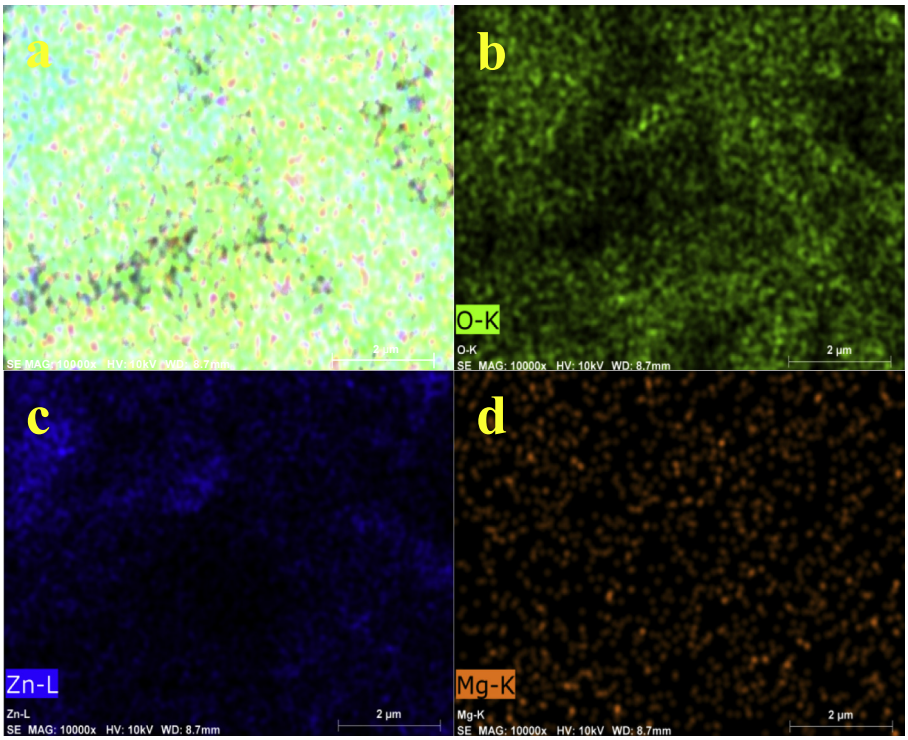

Fig. 4. Elemental mapping dots of 5 mol% Mg doped ZnO nanorod with (a) all elements (b) Zn − L series (c) O − K series and (d) Mg − K series.

Table 2
Electrical parameters calculated from Hall measurements.

Magnesium doping conc. in ZnO (mol%)	Carrier Concentration (cm^{-3})	Mobility ($cm^2\ V^{-1}\ s^{-1}$)	Resistivity (ohm-cm)	Type of Carrier
0	9.63×10^{15}	10.62	1365	*n*-type
5	3.80×10^{15}	4.904	1368	*n*-type
10	9.30×10^{14}	0.7475	2195	*n*-type
15	4.31×10^{14}	0.2944	2203	*n*-type

probability of the charge carriers. This increase in grain boundary scattering for charge transport reduced the conductivity and mobility. Carrier concentration of the samples is lessened due to Mg doping.

I–*V* characteristics were carried out on all the samples from −5 V to +5 V at room temperature with current limit set at 1 μA in the Keithley 2450 sourcemeter. We used a very small gold coated electrode clip which is in contact with the thin film for *I-V* measurements by standard four probe method. *I-V* is verified for its ohmic nature during both the cycles for its linearity and symmetry. *I-V* curve [Fig. 5] revealed the ohmic nature of the samples upon increasing the doping percentage. The current was found to decrease with an increase in Mg mole concentration. The number of injected carriers upon doping was very less when compared to the number of free carriers available in the ohmic region [41]. The reason behind this behaviour might be due to the creation of more number of defect states upon Mg doping. These defect states act as traps for the charge carriers during recombination and caused lesser number of injected carriers leading to decreasing current.

Fig. 6 shows the photoluminescence (PL) spectra of the nanorods. It depicted a sharp UV peak due to the recombination of free-exciton across the band gap which was called the near band edge emission (NBE). A minor broad visible emission, which is called deep level emission (DLE), was observed in the spectra. It was mainly due to the transition between defect levels. Because of the creation of too many non-radiative centres (or other loss mechanisms) after the diffusion of large number of Mg dopants, the cross section of the excitons and the exciton-exciton scattering probability were greatly reduced. Owing to this, the UV intensity in the PL spectra was diminished upon Mg doping [54]. Moreover, the UV intensity in PL was directly proportional to the crystallite size and the volume of the sample. Upon doping, the size (crystallite size *D*, *c/a* ratio and volume *V*) of the sample was decreased and so was the UV intensity [55]. The NBE emission was blue shifted from 3.18 eV to 3.26 eV upon doping leading to widening of bandgap. This could be attributed to the increase in Mg composition in the samples. The origin of this blue shift was not due to quantum confinement effect since the diameter of all the nanorod samples (mean diameter is from 80 to 114 nm) were far larger than the exciton Bohr radius (1.8 nm) of bulk ZnO [56]. Thus Mg doping should

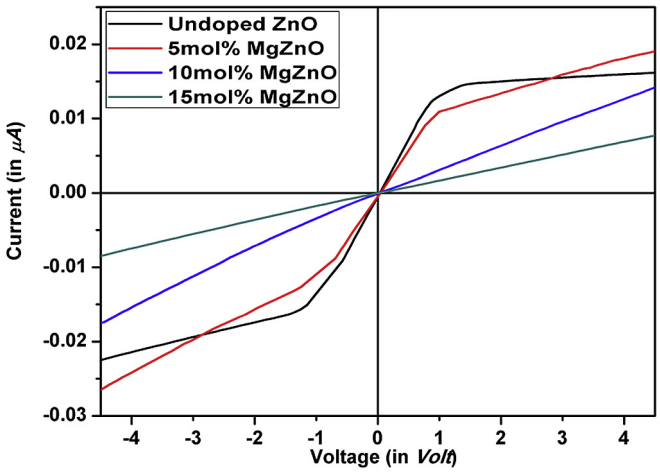

Fig. 5. Current-Voltage (*I-V*) curve of pure and Mg doped ZnO nanorods.

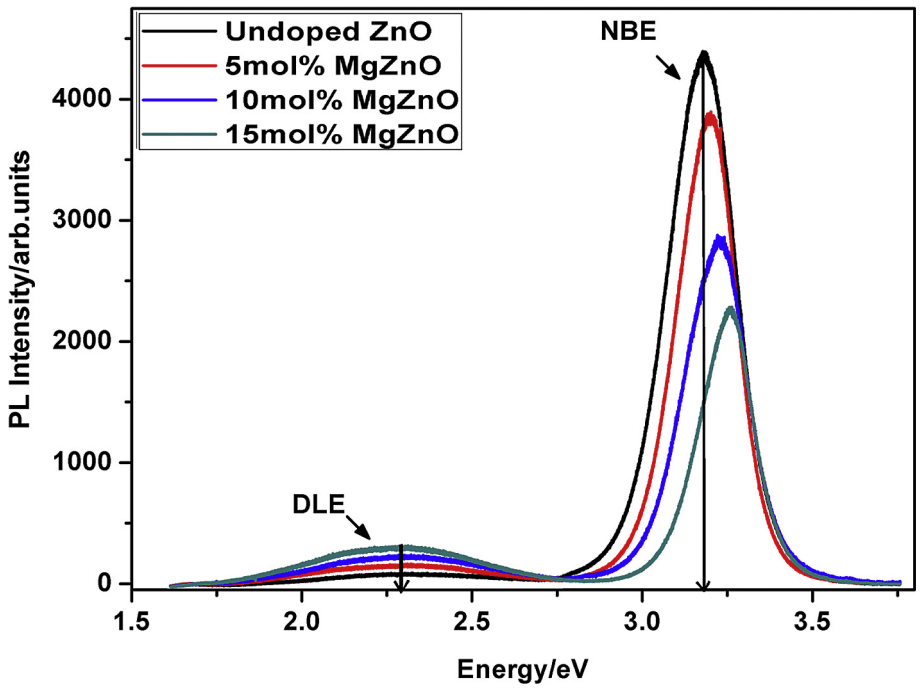

Fig. 6. Photoluminescence spectra of pure and MgZnO NRs.

be responsible for such a blue shift. PL spectra showed an increase in DLE upon doping which was due to the increase in defect states [57]. The deep level defects were responsible for this visible emission in ZnO [58]. The plausible candidate might be oxygen interstitial (O_i) which might exist in a doubly negative charge state especially in an *n*-type material [59]. The defect green emission occurred around 2.28 eV which was due to the presence of O_i according to the previous reports by H.Q. Wang et al. [60]. The electron mobility may get decreased in the presence of O_i, due to the ionized impurity scattering [61]. Hall measurements also revealed and confirmed the low mobility upon doping. Decrease in charge carrier concentration might be due to charge compensation at the acceptor states provided if there was any acceptor like defect such as O_i [62]. This was consistent with our observed results [Table 2].

To get further understanding of the recombination and transport of charges in terms of electrochemical processes, the electrochemical impedance spectroscopy (EIS) and cyclic voltammetry were used. 0.1 M NaOH aqueous solution was used as electrolyte in three electrode electrochemical cell in which the undoped, 5 mol%, 10 mol%, and 15 mol% MgZnO nanorods were used as working electrodes by keeping platinum electrode as counter electrode and Ag/AgCl as a reference electrode.

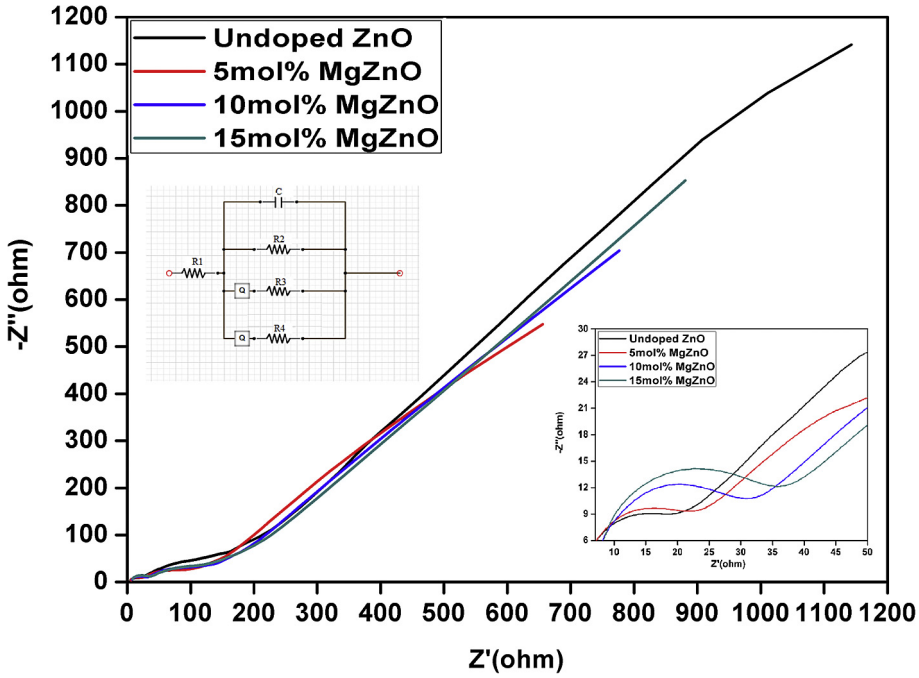

Fig. 7. Nyquist plot of undoped, 5 mol%, 10 mol%, and 15 mol% Mg doped ZnO nanorods in 0.1 M NaOH aqueous electrolyte solution. Inset shows the Nyquist plot in high frequency region along with the equivalent circuit.

EIS was done at the open circuit potential in the frequency ranging from 10 mHz to 100 KHz [Fig. 7]. The Nyquist plots were identical in shape and almost linear in the low frequency region. The semicircle part [inset of Fig. 7] in the high frequency region is associated with the charge transfer resistance. The arc radius is low in undoped ZnO and increases upon Mg doping. The total resistance (T_R) is calculated from the equivalent circuit by fitting the experimental data of Nyquist plots using ZSimpWin 3.22d software. The equivalent circuit [inset of Fig. 7] contains resistive (R), capacitive (C) and constant phase element (Q) in the combination of R((CR)[QR][QR]). From Table 3 it was clear that the undoped ZnO was having a minimum total resistance (T_R) of 998.21 Ω at the surface of the sample which facilitated faster interfacial charge transfer. Higher value of T_R in MgZnO NRs could stretch the pathway for charge transfer due to the effect of oxygen interstitial defect states. This increase in resistance might also be partly due to smaller pores of the MgZnO NRs resulting in pseudo capacitive behaviour. The smaller pores were expected to be more resistive in terms of ionic current flow through them. The transport mechanism explained in Hall measurements and *I-V* characterization studies agrees well with the observed results in EIS fitted parameters. Upon doping, the grain boundaries and the corresponding scattering might increase leading to decrease in electron conduction [63], which is consistent with our XRD and Hall measurement results.

The cyclic voltammetry measurements were performed at room temperature covering the potential range from −1.5 V to 0.6 V with a scan rate of 5, 25, 50 and 100 mV^{-1} [Fig. 8]. All the CV curves were having anodic and cathodic potentials (AP & CP), so the capacitive behaviour of these electrodes arouse due to redox mechanism. The area under the curve increased upon increasing the scan rate and redox peaks appeared at maximum current density. The redox reaction occurred due to the presence of depletion layer in the electrode/solution interface and external biasing. At a scan rate of 5 mV^{-1} more peaks were observed for undoped ZnO sample. So the dominance of redox mechanism observed mainly at lower scan rates. However in the doped samples the current density has been decreased even in lower scan rates compared to the undoped ZnO. This could be due to mechanism explained earlier like the increase in grain boundary scattering, smaller pore size of the samples etc. The larger surface area under the curve of undoped ZnO revealed higher current density with increased oxidation reaction compared to the doped samples. The availability of high electrochemically active sites caused by the surface hydroxylation of

Table 3
Total Resistance calculated from the equivalent circuit drawn from the fitted experimental parameters.

Magnesium doping conc. in ZnO (mol%)	R_1 (Ω)	R_2 (Ω)	R_3 (Ω)	R_4 (Ω)	Total Resistance (Ω) $T_R = R_1 + R_2 + R_3 + R_4$
0	4.52	777.8	15.49	200.4	998.21
5	4.72	1385	18.56	115.4	1523.68
10	6.47	6419	25.48	139.6	6590.55
15	6.65	8562	28.06	161.4	8758.11

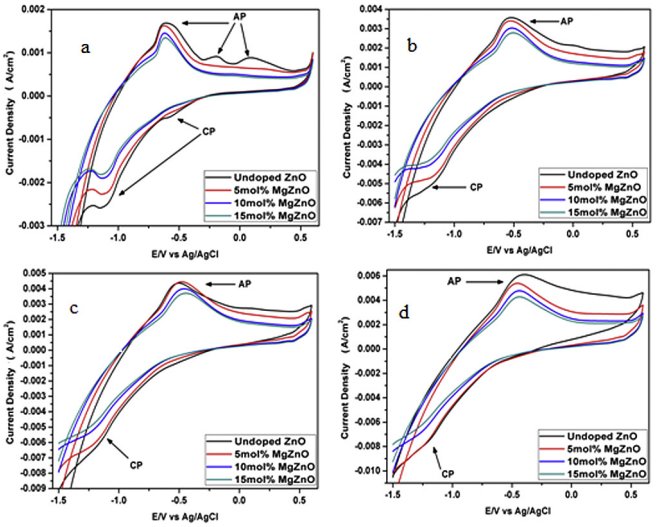

Fig. 8. Cyclic voltammograms of pure and MgZnO NRs recorded in 0.1 M NaOH at a scan rate of (a) 5 mV^{-1} (b) 25 mV^{-1} (c) 50 mV^{-1} and (d) 100 mV^{-1}.

pure ZnO enabled the active participation of all the nanorods in the entire surface. In the doped samples, there is a reduction of active sites. Undoped ZnO nanorod acting as electrode in an alkaline solution relied on the tunnelling of electron supplied from the electrode and OH^- ion diffusion in the host material. The decrease in pseudo capacitive performance of MgZnO samples could be attributed to (i) decreasing conductivity which affected the electron flow, (ii) reduced specific surface area of the electrode material and (iii) diminished interfacial charge transfer in between MgZnO nanorods and oxide-electrolyte interface.

4. Conclusion

The structural, optical and electrical properties were measured for undoped, 5 mol%, 10 mol%, and 15 mol% Mg doped ZnO nanorods grown by hydrothermal method. Due to amalgamation of Mg, replacing at the Zn matrix, resulted in the reduction of crystallite size and a shift in (002) peak. Accumulation of Mg at the boundary increases the grain boundary scattering. From FESEM images the diameters of the as-grown samples were found to be 80–114 nm. From the PL spectra we got the characteristic UV emission along with a defect emission around 2.28 eV. The spectra were blue shifted due to Mg doping. Since the diameters were well below the Bohr exciton radius (1.8 nm) this blue shift might be due to Mg doping. Oxygen interstitial (O_i) defect exists in the samples in doubly negative charge state. In the vicinity of O_i, the mobility gets decreased. The charge carrier concentration was decreased at the O_i state due to the occurrence of electron compensation. These results were confirmed by Hall and *I-V* measurements. Moreover from Hall measurements, the carrier type was found to be *n*-type in all the samples. The charge transfer resistance was measured from EIS for all the samples and found to increase upon Mg doping. This is due to smaller pores in the doped samples so that the charge carriers are finding themselves difficult to pass through. In cyclic voltammetry the redox mechanism has been observed and it was reduced when Mg was being incorporated. The reason for this behaviour might be smaller pore structure and decrease in specific surface area of the sample. Hence the structural modification and variation in the defect luminescence altered the electrical properties of the as-grown Mg doped ZnO nanorods. By suitably controlling the microstructure and defects we can improve the electrical properties of the magnesium doped zinc oxide nanorods for a specific application.

Acknowledgement

B. Santoshkumar thanks the UGC-SERO, Hyderabad for awarding the teacher fellowship under Faculty Development Programme vide F.No. FIP-TNMS039/001(TF)/PHYSICS/Ph.D/XII PLAN/2014-15 dated December 2014. Also he acknowledges the Solar Energy Research Laboratory, Dept. of Applied Physics and Dept. of Applied Chemistry, Indian Institute of Technology, Dhanbad for the facilities provided.

References

[1] S.M. Sultan, O.D. Clark, T.B. Masaud, Q. Fang, R. Gunn, M.M.A. Hakim, K. Sun, P. Ashburn, H.M.H. Chong, Microelectron. Eng. 97 (2012) 162.
[2] J.X. Wang, X.W. Sun, Y. Yang, H. Huang, Y.C. Lee, O.K. Tan, L. Vayssieres, Nanotechnology 17 (2006) 4995.
[3] Z.L. Wang, J. Phys. Condens. Matter 16 (2004) R829.
[4] T. Gao, T.H. Wang, Appl. Phys. A 80 (2005) 1451.

[5] L. Luoa, Y. Zhang, S.S. Mao, L. Lin, Sens. Actuators A 127 (2006) 201.
[6] J. Bao, M.A. Zimmler, F. Capasso, Nano Lett. 6 (2006) 1719.
[7] E.W. Seelig, B. Tang, A. Yamilov, H. Cao, R.P.H. Chang, Mater. Chem. Phys. 80 (2003) 257.
[8] Y. Dajani, I.A. Knize, Electron. Lett. 42 (2006) 1309.
[9] Adolfo A. Mosquera, David Horwat, Alexandr Rashkovskiy, Anatoly Kovalev, Patrice Miska, Dmitry Wainstein, Jose M. Albella, Jose L. Endrino, Sci. Rep. 3 (1714) (2013) 1.
[10] Min-Hua Zhao, Zhong-Lin Wang, Scott X. Mao, Nano Lett. 4 (4) (2004) 587.
[11] Hsu-Cheng Hsu, Ching-Sheng Cheng, Chia-Chieh Chang, Song Yang, Chen-Shiung Chang, Wen-Feng Hsieh, Nanotechnology 16 (2005) 297.
[12] A. Khorsand Zak, W.H. Abd. Majid, M.E. Abrishami, Ramin Yousefi, Solid State Sci. 13 (2011) 251.
[13] Ye Sun, N. George Ndifor-Angwafor, D. Jason Riley, Michael N.R. Ashfold, Chem. Phys. Lett. 431 (2006) 352.
[14] A. Chrissanthopoulos, S. Baskoutas, N. Bouropoulos, V. Dracopoulos, P. Poulopoulos, S.N. Yannopoulos, Photonics Nano. Fund. Appl. 9 (2011) 132.
[15] Xiang Liu, Xiaohua Wu, Hui Cao, R.P.H. Chang, J. Appl. Phys. 95 (6) (2004) 3141.
[16] A.L. Yang, H.Y. Wei, X.L. Liu, H.P. Song, G.L. Zheng, Y. Guo, C.M. Jiao, S.Y. Yang, Q.S. Zhu, Z.G. Wang, J. Cryst. Growth 311 (2009) 278.
[17] Sunandan Baruah, Joydeep Dutta, J. Sol-Gel Sci. Technol. 50 (2009) 456.
[18] Irene Gonzalez-Valls, Mónica Lira-Cantu, Phys. Procedia 8 (2010) 28.
[19] S. Yılmaz, E. Bacaksız, I. Polat, Y. Atasoy, Curr. Appl. Phys. 12 (2012) 1326.
[20] J.J. Hassan, M.A. Mahdi, Y. Yusof, H. Abu-Hassan, Z. Hassan, H.A. Al-Attar, A.P. Monkman, Opt. Mater 35 (2013) 1035.
[21] Minggang Zhao, Xinchang Wang, Jipeng Cheng, Liwei Zhang, Jianfeng Jia, Xinjian Li, Curr. Appl. Phys. 13 (2013) 403.
[22] A.H. Reshak, Sin Tee Tan, Fitri Yeni Naumar, A.A. Umar, M. Oyama, Z.A. Alahmed, H. Kamarudin, I.V. Kityk, Int. J. Electrochem. Sci. 9 (2014) 6352.
[23] Cheng-Liang Hsu, Hsieh-Heng Li, Ting-Jen Hsueh, ACS Appl. Mater. Interfaces 5 (2013) 11142.
[24] Wei Liu, Faxian Xiu, Ke Sun, Ya-Hong Xie, Kang L. Wang, Yong Wang, Jin Zou, Zheng Yang, Jianlin Liu, J. Am. Chem. Soc. 132 (2010) 2498.
[25] C. Torres-Torres, M. Trejo-Valdez, H. Sobral, P. Santiago-Jacinto, J.A. Reyes-Esqueda, J. Phys. Chem. C 113 (2009) 13515.
[26] S. Ilican, M. Caglar, Y. Caglar, Mater. Sci. Pol. 25 (3) (2007) 709.
[27] Kamakhya Prakash Misra, R.K. Shukla, Atul Srivastava, Anchal Srivastava, Appl. Phys. Lett. 95 (2009) 031901.
[28] Ming Gao, Jinghai Yang, Lili Yang, Yongjun Zhang, Jihui Lang, Huilian Liu, Hougang Fan, Yunfei Sun, Zhiqiang Zhang, Hang Song, Superlattices Microstruct. 52 (2012) 84.
[29] Yasemin Caglar, Kamuran Gorgun, Saliha Ilican, Mujdat Caglar, Fahrettin Yakuphanoglu, Appl. Phys. A 122 (733) (2016) 1.
[30] Te-Hua Fang, Shao-Hui Kang, J. Alloys Compd. 492 (2010) 536.
[31] J.R. Wang, Z.Z. Ye, J.Y. Huang, Q.B. Ma, X.Q. Gu, H.P. He, L.P. Zhu, J.G. Lu, Mater. Lett. 62 (2008) 1263.
[32] R.N. Gayen, S.N. Das, S. Dalui, R. Bhar, A.K. Pal, J. Cryst. Growth 310 (2008) 4073.
[33] Q.J. Wang, J.B. Wang, X.L. Zhong, Q.H. Tan, Z. Hu, Y.C. Zhou, Appl. Phys. Lett. 100 (2012) 132407.
[34] Parmod Kumar, Yogesh Kumar, Hitendra K. Malik, K. Asokan, AIP Conf. Proc. 1512 (2013) 990.
[35] Sanghyun Ju, Jianye Li, Ninad Pimparkar, Muhammad A. Alam, R.P.H. Chang, David B. Janes, IEEE Trans. Nanotechnol. 6 (3) (2007) 390.
[36] Y.H. Liu, S.J. Young, L.W. Ji, S.J. Chang, IEEE J. Sel. Top. Quantum Electron. 21 (4) (2015) 3800405.
[37] Jyun-Yi Li, Sheng-Po Chang, Ming-Hung Hsu, Tsung-Hsien Kao, Shoou-Jinn Chang, ECS J. Solid State Sci. Technol. 5 (7) (2016) Q191–Q194.
[38] Y.H. Liu, Sheng-Joue Young, C.H. Hsiao, Liang-Wen Ji, T.H. Meen, W. Water, Shoou-Jinn Chang, IEEE Photonics Technol. Lett. 26 (7) (2014) 645.
[39] Cheng-Zhi Wu, Liang-Wen Ji, Shi-Ming Peng, Yan-Lung Chen, Sheng-Joue Young, Electrochem. Solid-State Lett. 14 (9) (2011) J55–J57.
[40] A. Suryanarayana Reddy, P. Prathap, Y.P.V. Subbaiah, K.T. Ramakrishna Reddy, J. Yi, Thin Solid Films 516 (2008) 7084.
[41] B.K. Sonawane, M.P. Bhole, D.S. Patil, Mater. Sci. Semicond. Process. 12 (2009) 212.
[42] C.H. Hsu, D.H. Chen, Nanotechnology 21 (2010) 285603.
[43] R. Vettumperumal, S. Kalyanaraman, B. Santoshkumar, R. Thangavel, Mater. Res. Bull. 50 (2014) 7.
[44] B. Santoshkumar, S. Kalyanaraman, R. Vettumperumal, R. Thangavel, I.V. Kityk, S. Velumani, J. Alloys Compd. 658 (2016) 435.
[45] K.L. Chopra, S. Major, D.K. Pandaya, Thin Solid Films 102 (1983) 1.
[46] Jin Young Moon, Hyunghoon Kim, Ju Ho Lee, Jeong Yong Lee, Ho Seong Lee, Curr. Appl. Phys. 12 (2012) S52.
[47] A. Khorsand Zak, Ramin Yousefi, W.H. Abd Majid, M.R. Muhamad, Ceram. Int. 38 (2012) 2059.
[48] Rajkrishna Dutta, Nibir Mandal, Appl. Phys. Lett. 101 (2012) 042106.
[49] S. Kalyanaraman, R. Thangavel, R. Vettumperumal, J. Phys. Chem. Solids 74 (2013) 504.
[50] M.Z. Nursyahadah, Syahidah S. Nurul, Z. Azlan, Mahesh T. Kumar, AIP Conf. Proc. 1328 (2011) 211.
[51] R. Thangavel, Yia-Chung Chang, Thin Solid Films 520 (2012) 2589.
[52] Y.F. Li, B. Yao, Y.M. Lu, B.H. Li, Y.Q. Gai, C.X. Cong, Z.Z. Zhang, D.X. Zhao, J.Y. Zhang, D.Z. Shen, X.W. Fan, Appl. Phys. Lett. 92 (2008) 192116.
[53] K. Ip, Y.W. Heo, D.P. Norton, S.J. Pearton, J.R. LaRoche, F. Ren, Appl. Phys. Lett. 85 (2004) 1169.
[54] E.J. Guidelli, O. Baffa, D.R. Clarke, Sci. Rep. 5 (2015) 14004.
[55] K.E. Knutsen, A. Galeckas, A. Zubiaga, F. Tuomisto, G.C. Farlow, B.G. Svensson, A. Yu. Kuznetsov, Phys. Rev. B 86 (2012) 121203(R).
[56] A. Janotti, C.G. Van de Walle, Phys. Rev. B 76 (2007) 165202.
[57] Hsu-Cheng Hsu, Chun-Yi Wu, Hsin-Ming Cheng, Wen-Feng Hsieh, Appl. Phys. Lett. 89 (2006) 013101.
[58] W.Q. Peng, S.C. Qu, G.W. Cong, Z.G. Wang, Appl. Phys. Lett. 88 (2006) 101902.
[59] X.L. Wu, G.G. Siu, C.L. Fu, H.C. Ong, Appl. Phys. Lett. 78 (2001) 2285.
[60] M. Liu, A.H. Kitai, P. Mascher, J. Lumin. 54 (1992) 35.
[61] H.Q. Wang, G.Z. Wang, L.C. Jia, C.J. Tang, G.H. Li, J. Phys. D. Appl. Phys. 40 (2007) 6549.
[62] Emre Gür, G. Tabares, A. Arehart, J.M. Chauveau, A. Hierro, S.A. Ringel, J. Appl. Phys. 112 (2012) 123709.
[63] Yasuhiro Igasaki, Hiromi Saito, J. Appl. Phys. 70 (1991) 3613.